ORIGINAL PAPER

Linking the mechanical properties of frozen sandstone to phase composition of pore water measured by LF-NMR at subzero temperatures

Ting Wang[1] · Qiang Sun[1] · Hailiang Jia[2] · Juntong Ren[2] · Tao Luo[3]

Abstract

Water-bearing porous rocks can be greatly strengthened by freezing; its microscopic mechanisms lie in how subzero temperature modifies pore structure but have not yet been clearly defined. In this study, we link the mechanical properties of frozen sandstone to phase composition of pore water (i.e., relative amount of unfrozen water and ice). Both the strength (uniaxial compressive strength and tensile strength) and the phase composition of pore water (tested through the nuclear magnetic resonance (NMR) method) of frozen sandstone at nine subzero temperatures were measured. The results showed the following: (1) subzero temperature strengthened saturated sandstone significantly, both the strengths increased in a three-stage mode and each stage showed an approximately linear trend as temperature decreased from 0 to -20 °C; and (2) change of phase composition with freezing displayed two distinct stages: the rapid decreasing stage of unfrozen water content (0 to -4 °C), when bulk water and capillary water froze almost completely, and the slow decreasing stage (-4 to -20 °C), when adsorbed water froze partially. Based on direct observations on microscopic pore structure of sandstone and detailed discussion on the mechanical interactions between water, ice, and pore wall, phase composition may modify the mechanical properties of frozen rocks through the following effects: the supporting effect of ice under compression, the crack-filling effect of ice, the cementing effect of unfrozen water film under tension or under shearing load, and the frost damage effect. The former three are strengthening effects, while the latter one is weakening effect.

Keywords Frozen sandstone · Frozen strength · NMR · Phase composition · Microscopic mechanisms

✉ Hailiang Jia
  hailiang.jia@xust.edu.cn

  Ting Wang
  wangting@stu.xust.edu.cn

  Qiang Sun
  sunqiang04@cumt.edu.cn

  Juntong Ren
  584070506@qq.com

  Tao Luo
  luotao19870426@126.com

1 College of Geology and Environment, Xi'an University of Science and Technology, Xi'an 710054, Shaanxi Province, China

2 College of Architecture and Civil Engineering, Xi'an University of Science and Technology, No. 58 Yanta Middle Road, Xi'an 710054, Shaanxi Province, China

3 Key Laboratory of Safety and Durability of Concrete Structures of Shaanxi, Xijing University, Xi'an 710123, Shaanxi Province, China

Introduction

Understanding the mechanical properties of frozen rocks is fundamental for rock engineering in permafrost and polar regions (Jia et al. 2019). Mechanical properties of frozen rocks are sensitive to temperature change (Kodama et al. 2013; Atkinsona et al. 2018; Bai et al. 2020), estimating the influence of temperature change and revealing the mechanisms are of great significance for engineering design and protection (Shen et al. 2019), especially in the context of global warming (Gruber et al. 2004; Jia et al. 2017).

A number of studies have been conducted on the mechanical properties of frozen rocks; mechanical parameters including uniaxial compressive strength, tensile strength, elastic modulus, and fracture toughness have been tested under subzero temperatures (Dwivedi et al. 2000; Yamabe and Neaupane 2001; Glamheden and Lindblom 2002; Yang et al. 2010; Kodama et al. 2013; Weng et al. 2020). Freezing temperature, initial water content, loading rate, confining pressure, etc. have been regarded as major factors influencing the mechanical properties of frozen rocks

(Kodama et al. 2007; Atkinson et al. 2018; Jia et al. 2020; Kodama et al. 2019). Temperature, as one of the basic meteorological elements, is a key factor that determines whether a rock can freeze and to what extent it freezes (Kurilko and Novopashin 2005; Huang et al. 2018; Jia et al. 2019; Weng et al. 2019). Previous studies referring to the effect of freezing temperature have suggested the negative correlation between strength of frozen rocks and freezing temperature and commonly attribute this strengthening effect to pore ice (Atkinsona et al. 2018; Bai et al. 2020). However, due to the scarcity of data, generally 3~5 or even less subzero temperatures were adopted to test the mechanical properties of frozen rocks; the precise correlation between strength of frozen rocks and freezing temperature has not been revealed. Moreover, considering the fact that unfrozen water and ice coexist in pores of frozen rocks (Watanabe and Mizoguchi 2002; Vlahou and Worster 2010; Jia et al. 2020), attributing the strengthening effect of subzero temperature solely to pore ice should be biased. Here, we suggest that the phase composition of pore water at subzero temperatures, i.e., relative amount of unfrozen water and ice, and the interactions between each fraction determine the mechanical properties of frozen rocks.

Change of phase composition of pore water is a direct indictor of the freeze-thaw process of rock and soil. It is usually estimated by measuring unfrozen water content. Several methods, such as time-domain reflectometry (TDR), time-domain transmissometry (TDT), electrical resistivity tomography (ERT), ultrasonic testing, and low field nuclear magnetic resonance (LF-NMR) (Zhou et al. 2014; Yoshikawa and Overduin 2005; Brunet et al. 2010) have been employed, among which the LF-NMR method should be the most accurate since it measures the amount of hydrogen in liquid water directly. To investigate the linkage between mechanical properties of frozen rock and phase composition of pore water, mechanical parameters (uniaxial compressive strength, tensile strength, and deformability) of saturated sandstones at nine subzero temperatures were systematically tested. Phase compositions of pore water in saturated rocks at different subzero temperatures were measured using the LF-NMR method. Correlation between mechanical properties of frozen rocks and phase composition was revealed. Moreover, microscopic pore structure of used sandstone was observed through scanning electron microscope (SEM), based on which freezing pattern of pore water was analyzed. Microscopic mechanisms of phase composition determining frozen strength were discussed accordingly.

Experimental design

Sample preparations

Thirty-seven cylindrical specimens with a diameter of 50 mm and a length of 100 mm for the uniaxial compressive strength (UCS) test and thirty-two discal specimens with a diameter of

50 mm and a length of 25 mm for the Brazilian splitting test were drilled from the same fresh sandstone block. Aiming to further ensure the homogeneity of samples, P-wave velocities of the specimens were tested using an NM-4B ultrasonic tester. The T_2 spectrum of all water-saturated sandstones was tested by NMR. Thirty-one cylindrical specimens and twenty-seven discoid specimens that have similar P-wave velocities and T_2 spectrum (reflect the pore properties) were selected for mechanical and physical testing, respectively (Fig. 1a). All samples were numbered and the basic physical parameters of dry density, porosity, total pore water, and P-wave velocities were marked in Appendix Table 5. The average value of dry density, porosities, and P-wave velocities of the selected samples were 2.1 g/cm³, 19.58%, and 2.67 km/s, respectively.

The mean grain size of sandstone is 0.3 mm and the mineralogical properties (identified by X-ray diffraction) of the sandstone are summarized in Table 1.

All the selected samples were firstly dried at 105 °C for at least 48 h until their mass reached constant, and then placed in a vacuum chamber at − 1 bar for 4 h, and finally immersed in water for 72 h to achieve complete saturation. Afterwards, samples were wrapped with cling film and placed in a humidifier for 1 week to make the inner water distribution uniform.

Setups of experiments

Mechanical tests

The UCS tests and Brazilian tests were conducted using the WES-300B/600B testing machine. The test machine is equipped with a high-precision temperature-control chamber (Fig. 1b) which could provide subzero temperatures as low as − 30 °C with an accuracy of ± 0.1 °C.

Twenty-seven cylindrical specimens and discoid specimens were evenly divided into 9 groups respectively, corresponding to 9 testing temperatures, which were 0 °C, − 2 °C, − 4 °C, − 6 °C, − 8 °C, − 10 °C, − 12 °C, − 15 °C, and − 20 °C. Testing processes of the UCS tests and Brazilian tests were as follows: a saturated sample was firstly placed in the environmental chamber, set the temperature as a testing value. When the chamber temperature was achieved testing value, the sample was then frozen for 5 h (Fig. 2a) and maintained the testing value until the test finished. Afterwards, it was compressed or split to failure at an identical rate of 5 kN/min.

Measurement of the phase composition of sandstone at different temperatures

An NMR equipment was employed to measure the phase composition of pore water in sandstone at different subzero temperatures (Fig. 1c). The signal intensity of NMR is proportional to the number of water molecules (Watanabe and Wake
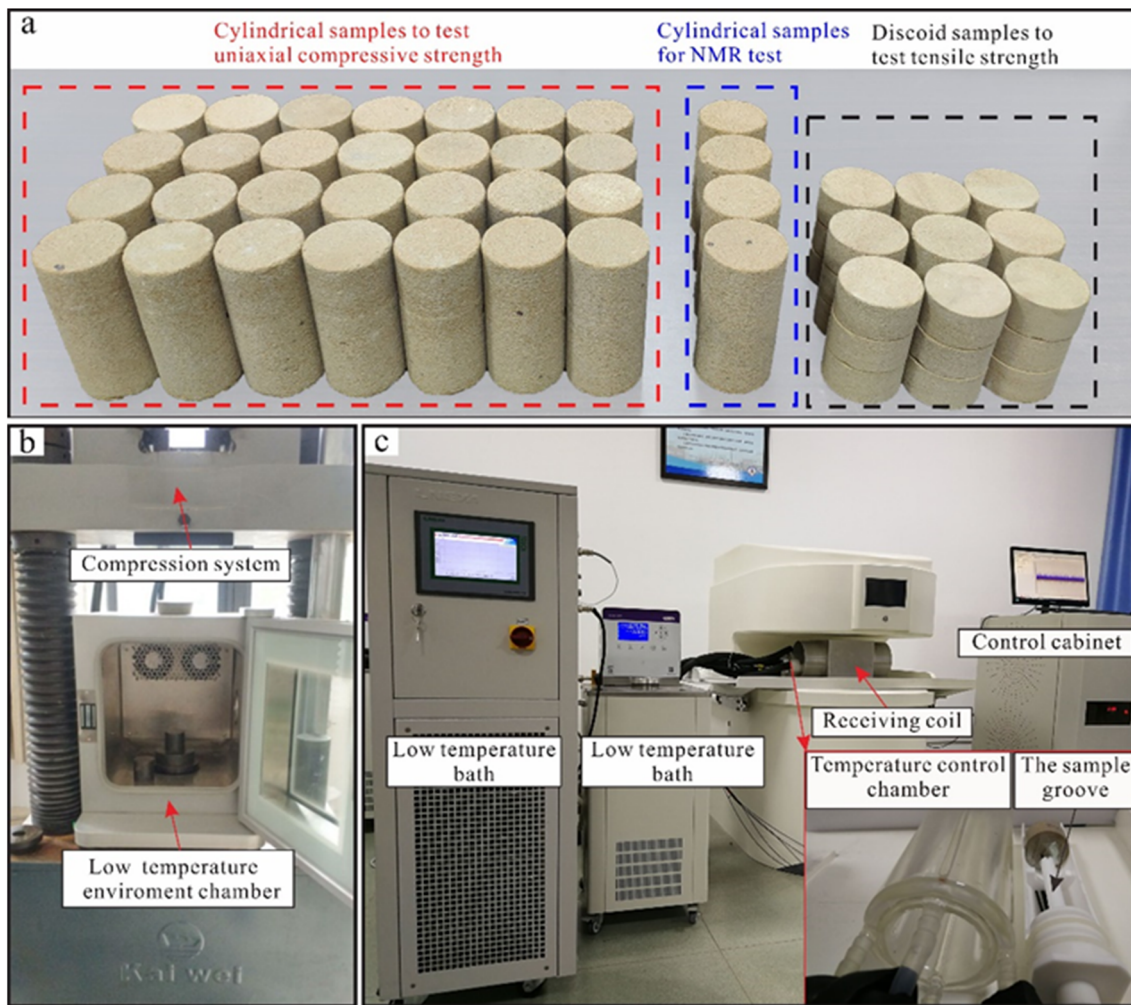
Fig. 1 Samples used in experiments (**a**), the uniaxial compression test system (**b**), and the NMR test system with an environmental chamber (**c**)

2009). At low magnetic fields, signals from ice can barely be detected (Zhao et al. 2017); therefore, the NMR signal can serve as an indicator of the unfrozen water in frozen rocks.

The NMR facility (MacroMR12-150H) used in our experiments was manufactured by Suzhou Niumag Analytical Instrument Corporation. An environmental chamber providing a uniform, three-dimensional freeze-thaw environment was integrated with the coil. The temperature inside the coil was controlled automatically by a software program; thus, the phase composition of the pore water was measured in real-time during freezing. The refrigerant fluid circulating through the environmental chamber was Fluorinert FC40. Both air temperature and

rock surface temperature inside the chamber were measured with optical fiber sensors.

Basic test parameters were as follows: static magnetic field intensity 0.3 T, echo time 0.18 ms, waiting time 2000 ms, echo numbers 1000, and numbers of scans 64. The Carr–Purcell–Meiboom–Gill (Carr and Purcell 1954; Meiboom and Gill 1958) pulse sequence was adopted. To achieve a uniformly distributed temperature field across the sample, ten temperature steps were preset (20 °C, 0 °C, − 2 °C, − 4 °C, − 6 °C, − 8 °C, − 10 °C, − 12 °C, − 15 °C, and − 20 °C), each consisting of a decreasing stage and a platform (Fig. 2b). The T_2 spectrum was measured every 15 min, each lasted for approximately 1 min.

Table 1 Mineral composition of sandstone

Mineral	Quartz	Kaolinite	Siderite	Microcline	Laumontite	Mica	Albite	Others
Content (%)	86.6	4.2	3.8	2.7	1	0.9	0.6	< 0.1

Fig. 2 Temperature regime used in uniaxial compressive and tensile strength test (**a**) and NMR test (**b**)
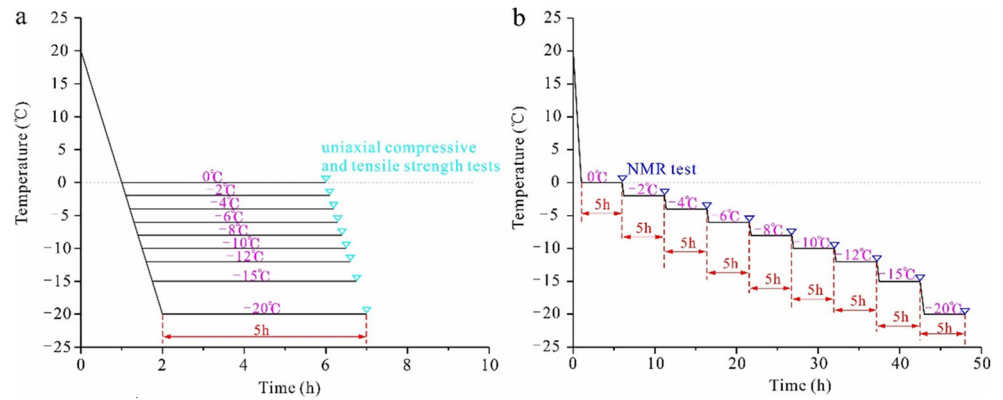
Results

Variation of mechanical properties with subzero temperatures

Stress-strain curves of the uniaxial compression tests

Freezing temperature had a significant effect on the stress-strain curves of saturated sandstone. The pre-peak stress-strain curves of frozen sandstone under uniaxial compression can be divided into the pore-compaction phase, elastic-deformation phase, and microcrack propagation phase (Fig. 3), which is similar to that of rock under positive temperatures. The lower the freezing temperature is, the higher the peak strength, failure strain, and elastic modulus under the same freezing time (5 h).

Variation of strength with subzero temperatures

When rock temperature decreased from 0 to − 20 °C, the UCS of saturated sandstones increased following a three-stage mode and each stage showed an approximately linear trend (Fig. 4a). The UCS of sandstone at − 20 °C was 3.3 times higher than that at room temperature. The average rate of
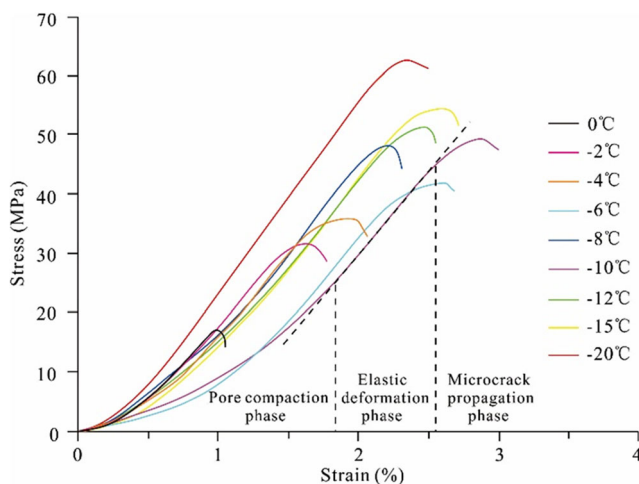

Fig. 3 Stress-strain curves of samples at different subzero temperatures

increase within each stage decreased. Within the first stage (temperature decreased from 0 to − 4 °C), the UCS increased by 16.7 MPa and the average rate of increase was 4.2 MPa/°C. When the temperature decreased from − 4 to − 12 °C (the second stage), the UCS increased by 16 MPa and the rate of increase was 1.9 MPa/°C. As the temperature decreased from − 12 to − 20 °C, the USC increased by 5.2 MPa and the rate of increase was 0.66 MPa/°C. The laws of UCS variation with temperature within each stage can be approximately expressed by Eq. 1. The fitting parameters "a" and "b" values of the formula of UCS changing with temperature at different temperature segments are showing Table 2.

$$\sigma_c = aT + b \tag{1}$$

The tensile strength of saturated sandstones changed with subzero temperature similarly to the UCS, following a three-stage mode as well (Fig. 4b). The tensile strength of sandstone at − 20 °C was 4.8 times higher than that at room temperature. The average rate of increase within each stage decreased. Within the first stage (temperature decreased from 0 to − 4 °C), the tensile strength increased by 1.6 MPa and the average rate of increase was 0.4 MPa/°C. When the temperature decreased from − 4 to − 10 °C (the second stage), the tensile strength increased by 0.67 MPa and the rate of increase was 0.11 MPa/°C. As the temperature decreased from − 10 to − 20 °C, the tensile strength increased by 0.4 MPa and the rate of increase was 0.04 MPa/°C. The laws of strength variation with temperature within each stage can be approximately expressed by Eq. 2. The fitting parameters "c" and "d" values of the

Table 2 The fitting parameters "a" and "b" values of the formula of UCS changing with temperature at different temperature segments

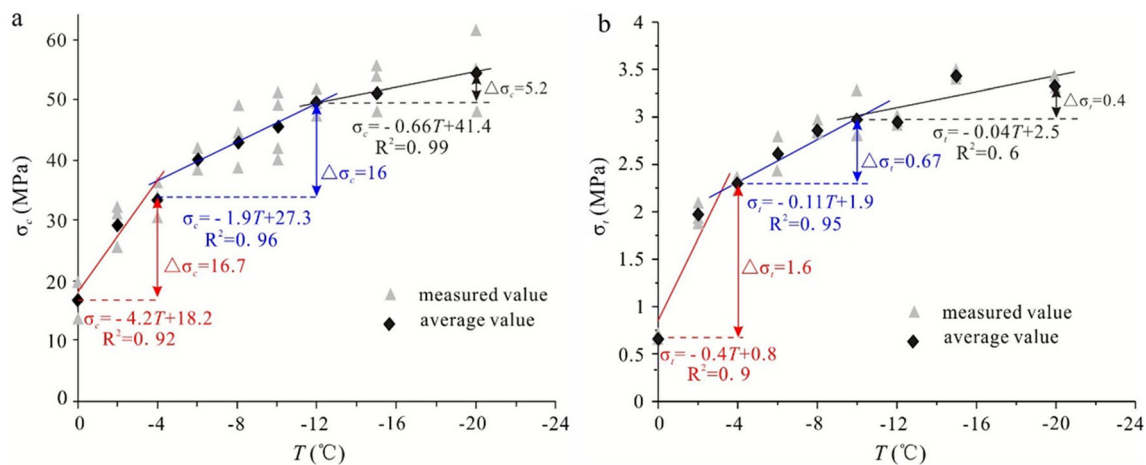| T (°C)	a (MPa/°C)	b (MPa)	R²
0°C≤T≤−4°C	− 4.2	18.2	0.92
−4°C≤T≤−12°C	− 1.9	27.3	0.96
−12°C≤T≤−20°C	− 0.66	41.4	0.99

Fig. 4 Strength of samples with different subzero temperatures showing **a** uniaxial compressive strengths (σ_c) and **b** tensile strengths (σ_t)

formula of tensile strength changing with temperature at different temperature segments are showed in Table 3.

$$\sigma_t = cT + d \tag{2}$$

Failure strain and elastic modulus under compression

The failure strain of saturated sandstones under compression first increased rapidly and then approached a steady value (Fig. 5a). The rapid-increase stage ended at around − 4 °C, where the failure strain increased by 2.2%. As temperature decreased from − 4 to − 20 °C, the failure strain approached a steady value of 2.4%. The failure strain of frozen sandstone at − 20 °C was 3.34 times higher than that at the room temperature. The elastic modulus increased approximately linearly from 26 to 33.8 GPa with rock temperature decreased from 0 to − 20 °C (Fig. 5b); this trend can be expressed by Eq. 3. The "e" and "f" are − 0.42 GPa/°C and 25 GPa, respectively.

$$E = eT + f \tag{3}$$

Variation of phase composition with subzero temperatures

T_2 is a time constant for the exponential decay of the magnitude of a spin echo (Cowan 1997) for a single pore body. For a

Table 3 The fitting parameters c and d values of the formula of tensile strength changing with temperature at different temperature segments

T (°C)	c (MPa/°C)	d (MPa)	R^2
0°C≤T≤−4°C	− 0.4	0.8	0.9
−4°C≤T≤−10°C	− 0.11	1.9	0.95
−10°C≤T≤−20°C	− 0.04	2.5	0.6

multiple pore body system such as a porous network, the exponential decay is a summation of the individual decays. Using an inversion processing technique, the raw decay curve can be fitted to a T_2 spectrum. Most of the NMR interpretations and estimated petro-physical parameters are based on this T_2 spectrum (Dastidar 2007).

The relative unfrozen water content of each sample was calculated using Eq. 4:

$$S_r = \frac{A_{T_2}^{frozen}}{A_{T_2}^{initial}} *100 \tag{4}$$

where, S_r is the normalized unfrozen water content of a specimen; $A_{T_2}^{frozen}$ is the T_2 area of the specimen frozen at a subzero temperature; and $A_{T_2}^{initial}$ is the T_2 area of the specimen at 0 °C. The above values were calibrated to eliminate the effect of temperature on NMR signals with the method proposed by Tice et al. (1982).

Variation of T_2 spectrum and unfrozen water content

The T_2 spectrum of saturated sandstone before freezing had three distinct peaks. With the decrease of temperature, the T_2 spectrum shifted leftwards and its area firstly decreased significantly (0~− 4 °C) and then slowly (− 4~− 20 °C) (Fig. 6a). We calculated the unfrozen water content at different subzero temperatures according to Eq. 4, the results are shown in Fig. 6b. As one can expect, the unfrozen water content first decreased rapidly (0~− 4 °C) and then slowly (− 4~− 20 °C) with the decrease of temperature.

As rock temperature decreased from 0 to − 2 °C, peak 3 and peak 2 lowered significantly. The − 4 °C was a turning point where peak 2 became negligible and peak 3 disappeared completely, indicating the freezing of bulk water and capillary water, while peak 1 reduced remarkably as
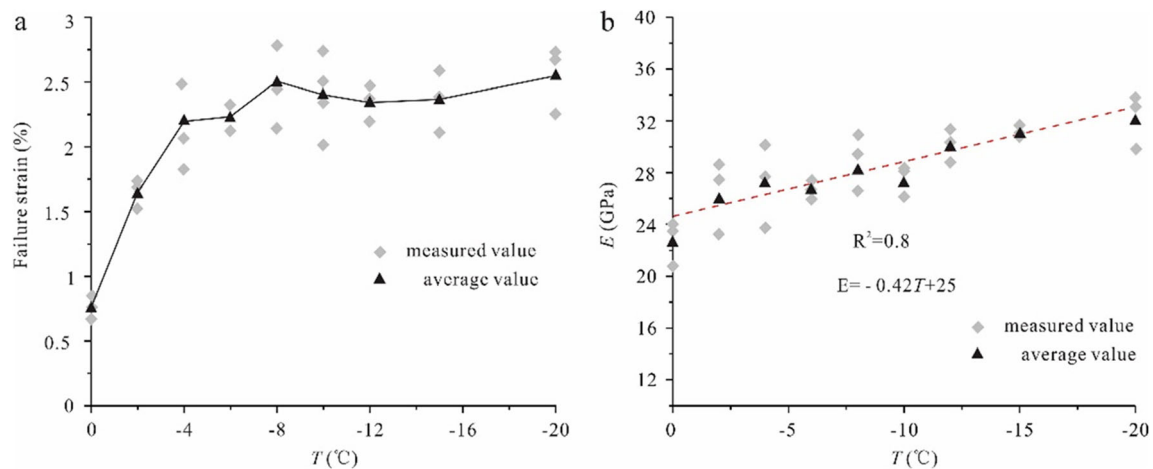
Fig. 5 Failure strain (**a**) and elastic modulus (E) (**b**) of samples at different subzero temperatures

well. When rock temperature got below − 4 °C, peak 1 shrunk slowly.

Variation of each fraction of pore water during freezing

Regarding the confinement of pore water in porous rocks, it can be broadly categorized into three types: bound water, capillary water, and bulk water (or free water) (Coates et al. 1998). Fractions of pore water can be deduced from the T_2 spectrum (Godefroy et al. 2001). The T_2 of bound water in sandstone is generally < 3 ms, that of capillary water is between 3 and 33 ms, and T_2 greater than 33 ms is associated with bulk water (Matteson et al. 1998; Martinez and Davis 2000). The above two critical values to partition pore water fractions in the present study were employed.

Variation of each fraction during freezing differed (Fig. 7). At early stage of freezing (0~− 4 °C), the content of bulk water and capillary water dropped to near zero at − 4 °C, while the content of adsorbed water firstly increased (0~− 2 °C) then decreased rapidly (− 2~− 4 °C). As rock temperature

decreased below − 4 °C, the adsorbed water froze slowly and its amount finally tend to be stable.

Discussion

Correlating strength of frozen sandstone with phase composition

Both strengths of frozen sandstone had a piecewise-linear correlation with phase composition (employing relative ice content I_r calculated with $I_r = 100 − S_r$ as the variable, unfrozen water content is equivalent) of pore water, as shown in Fig. 8.

The UCS of frozen sandstone increased with I_r following a two-stage mode and each stage showed an approximately linear trend (Fig. 8a). Within the first stage (I_r increased from 0 to 88.5%), the average increase rate of UCS was 0.183 MPa/%, while within the second stage (I_r increased from 88.5% to 95.8%), the average increase rate was 2.75 MPa/%, much higher than in the first stage. Correlation between the UCS
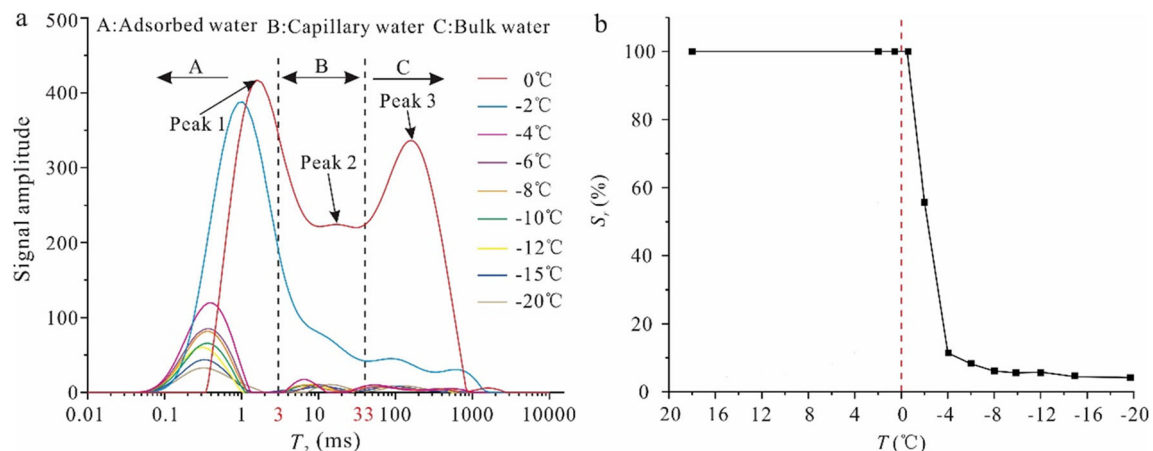

Fig. 6 Variation in T2 spectrum (**a**) and unfrozen water content (**b**) of samples with rock temperatures
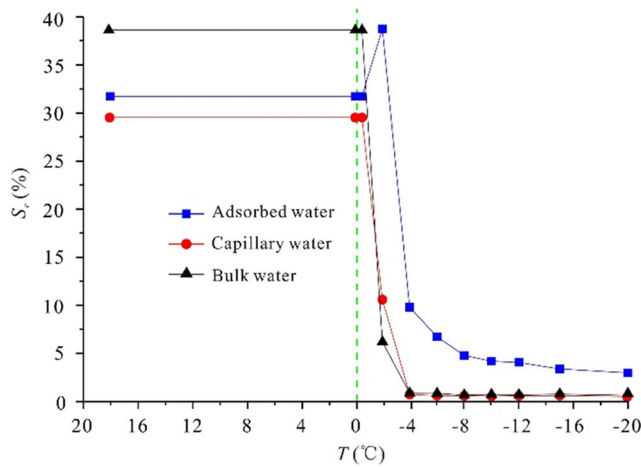
Fig. 7 Variation in each fraction of pore water in saturated sandstone with different temperatures

of frozen sandstone and I_r can be expressed by Eq. 5.

$$\sigma_c = gI_r + h \tag{5}$$

where, "g" and "h" are linear fitting parameters. The tensile strength of frozen sandstone changed with I_r following a two-stage mode as well (Fig. 8b). As the I_r increased from 0 to 88.5% (first stage), the average increase rate of tensile strength was 0.018 MPa/%; as I_r increased from 88.5% to 95.8%, the average increase rate was 0.15 MPa/%, 8.3 times as fast as in the first stage. Correlation between the tensile strength of frozen sandstone and I_r can be expressed by Eq. 6.

$$\sigma_c = jI_r + k \tag{6}$$

where, "j" and "k" are linear fitting parameters. Values of "g", "h", "j", and "k" are listed in Table 4.

Considering the high values of R^2 (> 0.8) in all fitting equations (Table 4), the piecewise-linear correlation between strength of frozen sandstone and phase composition of pore water is authentic. The temperature − 4 °C is the inflection point of the above piecewise-linear correlation (Fig. 8), which

is also an inflection point of phase composition variation (Fig. 6b). This on one hand confirms the correlation between strength of frozen sandstone and phase composition, and on the other hand provides some clues to mechanism analysis on phase composition determining frozen strength.

Pore structure of sandstone and freezing mode of pore water

Pores are the space where water and ice stay; pore structure has a significant influence in phase transition of water. Aiming to reveal the intrinsic relationship between the phase composition and the mechanical properties of frozen rocks, the pore structure should be observed first. The SEM (scanning electron microscopy) method was used to explore pore structure of used sandstone; the result is shown in Fig. 9. Pores in sandstone consist of macropores (diameter > 0.1 mm), mesopores (diameter between 2 μm and 0.1 mm), and micropores (diameter < 2μm) (Ondrášik and Kopecký 2014), and have good connectivity (Fig. 9a, b). Abstracted pore structure of sandstone is shown in Fig. 9c.

Based on the abstracted pore structure model, the freezing mode of pore water was analyzed. Bulk water exists in macropores and gravity controls its movement; capillary water exists primarily in mesopores and suffers from capillary pressure, adsorbed water exists both in the micropores and on the surface of mineral grains (i.e., the pore wall) and endures the largest binding force (Fig. 10a). According to the Clapeyron equation, the freezing point of water is negatively correlated with pressure (De Groot and Mazur 2013). Consequently, bulk water, capillary water, and adsorbed water freeze successively.

As temperature decreased from 0 to − 4 °C, bulk water, capillary water, and a part of adsorbed water froze. In this process, the volume expansion during water-ice phase transition expanded the pore space (Colbeck 1982; Matsuoka and Murton 2008). As a result, new micropores were generated
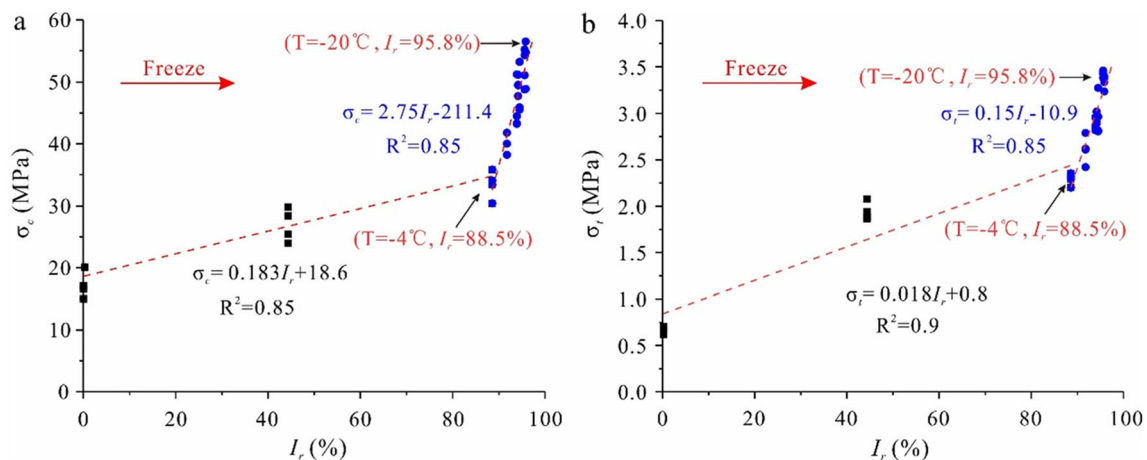

Fig. 8 Variation in rock strength with different ice content and **a** uniaxial compressive strength (σ_c) and **b** tensile strength (σ_t) of samples

Table 4 Values of the fitting parameters "g", "h", "j", and "k" in Eqs. (5) and (6)

I_r	σ_c			σ_t		
	g (MPa)	h (MPa)	R^2	j (MPa)	k (MPa)	R^2
$0 \leq I_r \leq 88.5$	0.183	18.6	0.85	0.018	0.8	0.9
$0.885 \leq I_r \leq 95.8$	2.75	− 211.4	0.85	0.15	− 10.9	0.85

and a portion of unfrozen water was pushed into them (Fig. 10b), which contributes to the temporary increase of adsorbed water content (Fig. 7). At − 4 °C, 89% of the total pore water had frozen (Figs. 6b and 7), and unfrozen water was adsorbed water. With temperature continually decreasing, adsorbed water either in smaller micropores or sandwiched between ice and pore wall froze further (Fig. 10c), resulting in growth of pore ice (Fig. 10c1) and thinning of unfrozen water film (Fig. 10c2) (Dash et al. 2006; Rempel 2007).

Microscopic mechanisms of phase composition determining frozen strength

As discussed above, phase composition of pore water covers on one hand the relative amount of unfrozen water and ice and on the other hand the mechanical interactions between water, ice, and rock skeleton. Considering the interactions between the above three phases under external load, phase composition may modify the mechanical properties of frozen rocks through the following effects.

(i)   The supporting effect of ice under compression (Fig. 11, *strengthening effect I*), pores tend to close under compression, pore ice provides supporting force and thus increases compressive strength and modulus of frozen rocks. The supporting effect could be enhanced by decreasing subzero temperatures since mechanical properties of ice increase with decreasing subzero temperatures.

(ii) The crack-filling effect of ice (Fig. 11, *strengthening effect II*), with reference to fracture mechanics, stress concentrates at crack tips under external load, which causes the crack to propagate more easily. Degree of stress concentration is usually measured by the stress intensity factor which is positively correlated to the crack length. As pore ice fills the cracks, its length becomes shorter, effectively reducing the stress concentration at crack tips. Therefore, the crack-filling effect strengthens frozen rocks. The crack-filling effect is controlled by size of pore ice and thus has a negative correlation with decreasing subzero temperatures.

(iii) The cementing effect of unfrozen water film under tension or under shearing load (Fig. 11, *strengthening effect III*), pore walls are adhered to ice by unfrozen water film, the resistance to tension and shear failure of the pore is thereby increased. The adhesive force of unfrozen water film is primarily controlled by its thickness, which is further determined by the freezing temperature (Guerin et al. 2016; Chen et al. 2018). The relationship between the adhesive force and temperature can be expressed in Eq. (7):

$$\Delta P = \frac{2\gamma[\cos(\theta_i) + \cos(\theta_s)]}{a - b \log(T_f - T_a)} \tag{7}$$

where, ΔP is the adhesive force, MPa; γ is the surface tension of the water (N/m); θ_i is the contact angle between ice crystals and the unfrozen water film; θ_s is the contact angle between the unfrozen water film and the rock; T_f is the fusion temperature of ice; T_a is the air temperature during precipitation; $a = 32$ nm and $b = 21$ nm. The above relationship is applicable within the temperature interval of 0∼− 12 °C, below the adhesive force gradually decreases (Jellinek 1959).

(iv) The frost damage effect (Fig. 11, *weakening effect I*), during the freezing of pore water, volumetric expansion exerts frost heaving force to pore walls leading to the expansion of existing pores and generation of new micropores. In other words, rock skeleton is damaged and mechanical properties of frozen rock are weakened (Jia et al. 2020).
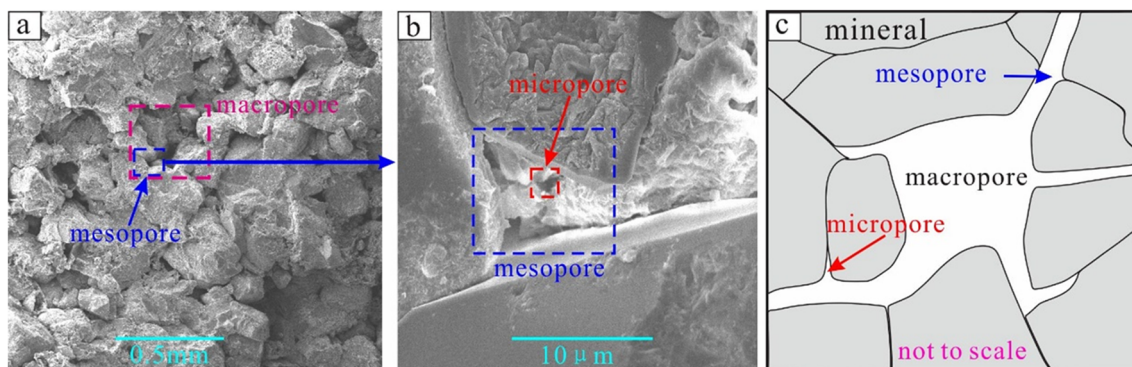

Fig. 9 Pore structure of sandstone observed via scanning electron microscope (SEM) magnified by 25 times (**a**) and 1000 times (**b**), and the abstracted pore structure model (**c**)
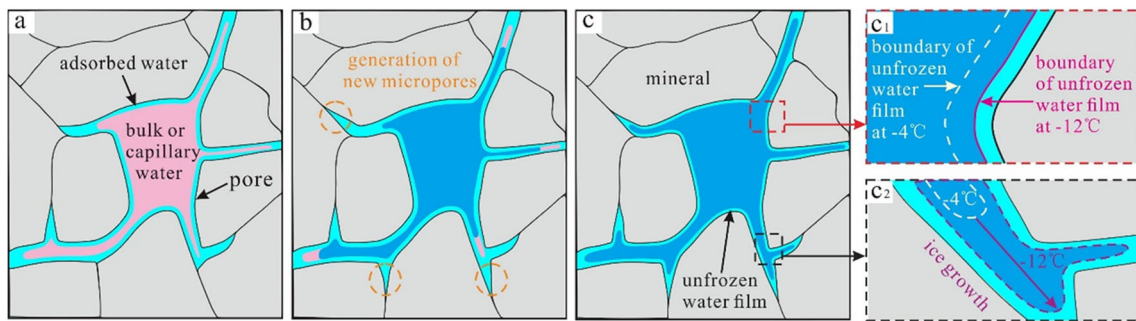
Fig. 10 Freezing process of saturated sandstone **a** initial saturated state; **b** freeze of bulk water, capillary water, and partially absorbed water; and **c** freeze of absorbed water within unfrozen water film (**c1**) and small pores (**c2**)

The level of volumetric expansion-induced damage is proportional to the volume of water that freezes; it has an inverse correlation with decreasing subzero temperatures.

The above four effects work simultaneously during freezing of pore water and shape the variation tendency of strength of frozen rocks with freezing temperature.

Fig. 11 Microscopic mechanisms of phase composition determining frozen strength

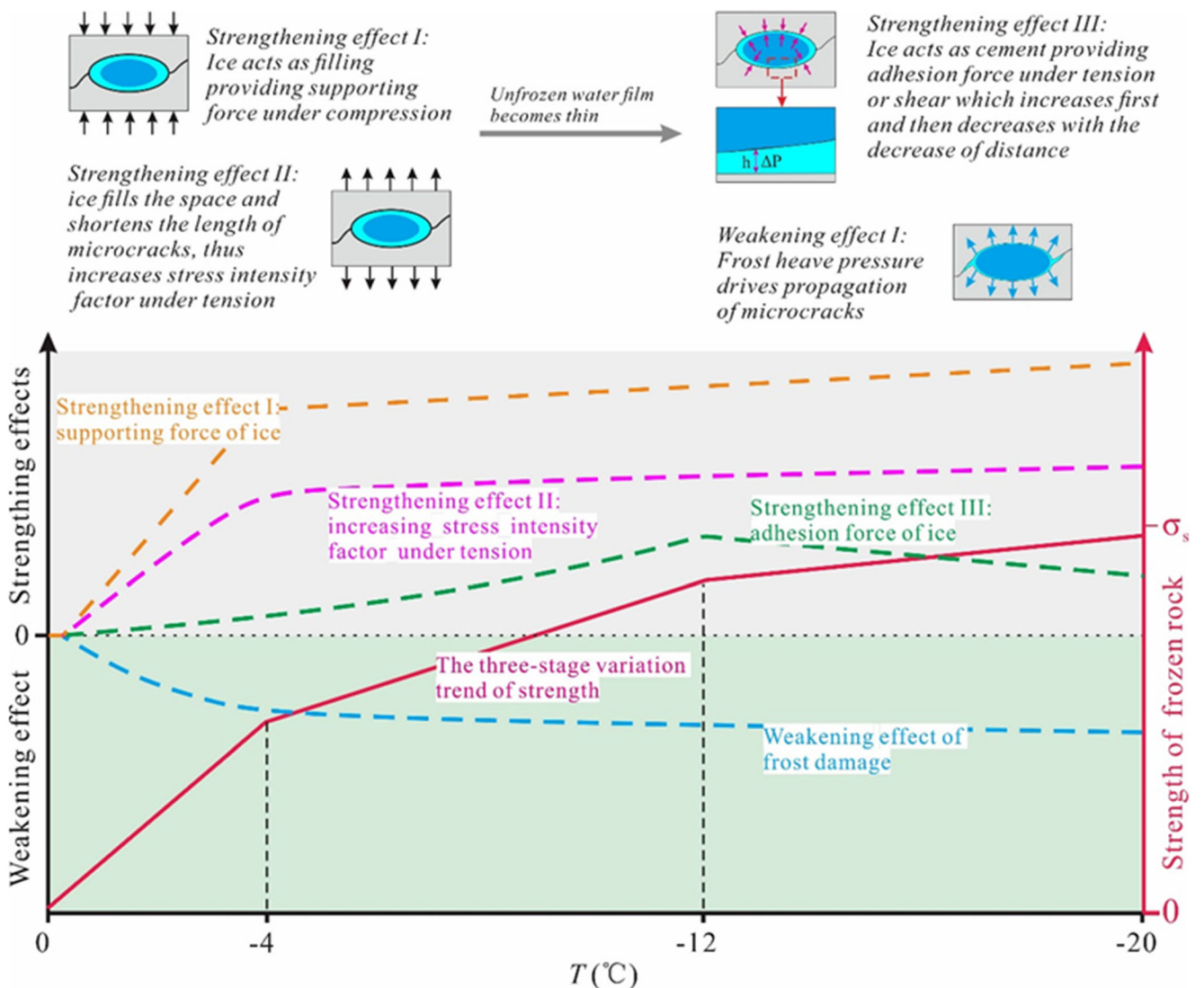During the first stage of freezing (0 to − 4 °C), rock strength increased rapidly (Fig. 4), meanwhile, the majority of pore water froze (Figs. 6 and 7), pore ice grew remarkably (Fig. 10). This implies that all the above four effects worked at this stage and three strengthening effects suppressed the weakening effect, resulting in a rapid increase in rock strength (Fig. 11). As temperature decreased further to − 12 °C, strength of frozen rocks still increased but with a lower rate (Fig. 4), only a bit of adsorbed water froze (Figs. 6 and 7), the volume of pore ice changed little (Fig. 10), thus *strengthening effect I and II* became insignificant (Fig. 11). While the *strengthening effect III* dominated the increase of strength due to the enlargement of the adhesive force between ice and pore walls (Fig. 11). When temperature dropped below − 12 °C, rock strength continued to increase but with an even lower rate (Fig. 4). Within this temperature interval, the *strengthening effect III* still dominated the increase of strength; however, the effect itself became weaker because of the decrease of the adhesive force between ice and pore walls (Fig. 11).

Conclusion

In this study, we tested both the mechanical properties of frozen sandstone and phase composition of pore water at a number of subzero temperatures. Correlations between mechanical properties of frozen rocks and phase composition and the microscopic mechanisms were analyzed, based on direct observations on microscopic pore structure of used sandstone through SEM and detailed discussion on the mechanical interactions between water, ice, and pore walls. According to the above results and analysis, we drew the following conclusions:

(1) Subzero temperature strengthened saturated sandstone significantly, both the UCS and tensile strength increased in a three-stage mode and each stage showed an approximately linear trend as rock temperature decreases from 0 to − 20 °C; failure strain and elastic modulus of frozen sandstone increased as well. The UCS and tensile strength at − 20 °C was 3.3 and 4.8 times higher than that at 0 °C

(2) Change of phase composition with freezing displayed two distinct stages. When temperature decreased from 0 to − 4 °C, the unfrozen water content decreased by 88.5% but merely by 7.3% as temperature decreased further from − 4 to − 20 °C. At the rapid decreasing stage of unfrozen water content (0 to − 4 °C), bulk water, capillary water, and most of adsorbed water froze, while at the slow decreasing stage (− 4 to − 20 °C), a portion of remained adsorbed water froze.

(3) Strength of frozen sandstone had a piecewise-linear correlation with the relative ice content. Considering the high values of R-square (> 0.9) in all fitting equations, the piecewise-linear correlation between strength of frozen sandstone and phase composition of pore water is authentic.

(4) Pores in sandstone consist of macropores, mesopores, and micropores, and have good connectivity. As temperature decreased from 0 to – 4 °C, the volumetric expansion during water-ice phase transition expanded the pore space, as a result, new micropores were generated and a portion of unfrozen water was pushed into them. At – 4 °C, 89% of the total pore water had frozen, and unfrozen water was adsorbed water. With temperature continually decreasing, adsorbed water either in smaller micropores or sandwiched between ice and pore wall froze further, resulting in growth of pore ice and thinning of unfrozen water film.

(5) The phase composition of pore water and the interactions between each fraction determine the mechanical properties of frozen sandstone. Considering the interactions between the above three phases under external load, phase composition may modify the mechanical properties of frozen rocks through the following effects: the supporting effect of ice under compression, the crack-filling effect of ice, the cementing effect of unfrozen water film under tension or under shearing load, and the frost damage effect. The former three are strengthening effects, while the latter one is weakening effect.

(6) The above four effects work simultaneously during freezing of pore water and shape the variation tendency of strength of frozen rocks with freezing temperature. When temperature of rock was between 0 and − 4 °C, three strengthening effects suppressed the weakening effect, resulting in a rapid increase in rock strength. As rock temperature decreased to − 12 °C, *strengthening effect III* dominated the increase of strength due to the enlargement of the adhesive force between ice and pore walls. With temperature decreasing further, the *strengthening effect III* still dominated the increase of strength; however, the effect itself became weaker.

Appendix. Physical parameters of samples used in this research

Table 5 Physical parameters of samples

	Number	Dry density (g/cm^3)	Porosity (%)	Total pore water (g)	P-wave velocity (km/s)
UCS test	1	2.08	19.56%	36.01	2.67
	2	2.08	19.68%	36.06	2.65
	3	2.11	19.96%	37.24	2.63
	4	2.09	19.23%	35.51	2.78
	5	2.11	19.64%	35.95	2.64
	6	2.09	19.25%	35.27	2.74
	7	2.10	19.56%	36.34	2.65
	8	2.09	19.78%	36.74	2.63
	9	2.10	19.43%	35.83	2.74
	10	2.11	19.79%	36.80	2.69
	11	2.10	19.59%	36.10	2.71
	12	2.11	19.37%	35.74	2.70
	13	2.11	19.48%	36.33	2.68
	14	2.12	19.69%	36.30	2.67
	15	2.12	19.61%	36.11	2.63
	16	2.11	19.16%	35.60	2.73
	17	2.10	19.71%	36.46	2.68
	18	2.11	19.45%	35.91	2.73
	19	2.12	19.63%	36.04	2.66
	20	2.08	19.71%	36.38	2.60
	21	2.09	19.30%	35.68	2.75
	22	2.11	19.78%	36.29	2.63
	23	2.08	19.88%	37.11	2.62
	24	2.08	19.91%	36.69	2.64
	25	2.10	19.55%	36.58	2.74
	26	2.11	19.35%	35.96	2.73
	27	2.09	19.43%	35.66	2.67
NMR test	1	2.09	19.85%	36.52	2.66
	2	2.11	19.49%	36.32	2.63
	3	2.09	19.34%	35.53	2.65
	4	2.10	19.69%	36.59	2.67
TS test	1	2.10	19.52%	8.99	2.65
	2	2.11	19.73%	9.04	2.68
	3	2.11	19.61%	9.15	2.75
	4	2.09	19.56%	9.03	2.63
	5	2.10	19.59%	8.96	2.65
	6	2.10	19.63%	8.99	2.67
	7	2.08	19.68%	9.14	2.73
	8	2.10	19.56%	9.08	2.74
	9	2.11	19.43%	8.96	2.67
	10	2.12	19.69%	9.15	2.64
	11	2.10	19.67%	9.06	2.74
	12	2.10	19.49%	8.99	2.67
	13	2.11	19.56%	9.12	2.65
	14	2.12	19.34%	8.91	2.66

Table 5 (continued)

Number	Dry density (g/cm³)	Porosity (%)	Total pore water (g)	P-wave velocity (km/s)
15	2.08	19.56%	9.00	2.70
16	2.10	19.71%	9.15	2.65
17	2.11	19.45%	9.00	2.67
18	2.10	19.61%	9.05	2.63
19	2.12	19.78%	9.08	2.73
20	2.11	19.65%	9.07	2.68
21	2.10	19.73%	9.12	2.73
22	2.10	19.56%	8.97	2.66
23	2.11	19.49%	9.09	2.60
24	2.09	19.57%	9.01	2.75
25	2.09	19.46%	9.10	2.63
26	2.09	19.60%	9.11	2.65
27	2.10	19.56%	8.98	2.71

References

Atkinson J, Durhama WB, Seagera S (2018) The strength of ice-saturated extraterrestrial rock analogs. Icarus 315:61–68. https://doi.org/10.1016/j.icarus.2018.06.016

Bai Y, Shan RL, Ju Y, Wu YX, Sun PF, Wang ZE (2020) Study on the mechanical properties and damage constitutive model of frozen weakly cemented red sandstone. Cold Reg Sci Technol 171: 102980. https://doi.org/10.1016/j.coldregions.2019.102980

Brunet P, Clément R, Bouvier C (2010) Monitoring soil water content and deficit using electrical resistivity tomography (ERT)—a case study in the Cevennes area, France. J Hydrol 380:146–153. https://doi.org/10.1016/j.jhydrol.2009.10.032

Carr HY, Purcell EM (1954) Effects of diffusion on free precession in nuclear magnetic resonance experiments. Phys Rev 94:630–638. https://doi.org/10.1103/PhysRev.94.630

Chen HX, Wu YC, Xia HY, Jing BY, Zhang QJ (2018) Review of ice-pavement adhesion study and development of hydrophobic surface in pavement deicing. J Traffic Transport Eng (Engl Ed) 5:224–238. https://doi.org/10.1016/j.jtte.2018.03.002

Coates GR, Galford J, Mardon D, Marschall D (1998) A new characterization of bulk-volume irreducible using magnetic resonance. Log Anal 39(1):51–63

Colbeck SC (1982) Configuration of ice in frozen media. Soil Sci 133(2): 116–123. https://doi.org/10.1097/00010694-198202000-00005

Cowan BP (1997) Nuclear magnetic resonance and relaxation. Cambridge University Press, Cambridge

Dash JG, Rempel AW, Wettlaufer JS (2006) The physics of premelted ice and its geophysical consequences. Rev Mod Phys 78(3):695–741. https://doi.org/10.1103/RevModPhys.78.695

Dastidar R (2007) Nuclear magnetic resonance (NMR) study of freezing and thawing of saturated porous media and application to shale and pore volume compressibility estimation. Dissertation, University of Oklahoma

De Groot SR, Mazur P (2013) Non-equilibrium thermodynamics. Courier Corporation, Massachusetts

Dwivedi RD, Soni AK, Goel RK, Dube AK (2000) Fracture toughness of rocks under sub-zero temperature conditions. Int J Rock Mech Min Sci 37(8):1267–1275. https://doi.org/10.1016/S1365-1609(00)00051-4

Glamheden R, Lindblom U (2002) Thermal and mechanical behaviour of refrigerated cavernsin hard rock. Tunn Undergr Space Technol 17(4):341–353. https://doi.org/10.1016/S0886-7798(02)00029-9

Godefroy S, Korb JP, Fleury M, Bryant RG (2001) Surface nuclear magnetic relaxation and dynamics of water and oil in macroporous media. Phys Rev E 64:021605. https://doi.org/10.1103/PhysRevE.64.021605

Gruber S, Hoelzle M, Haeberli W (2004) Permafrost thaw and destabilization of Alpine rock walls in the hot summer of 2003. Geophys Res Lett 31:L13504. https://doi.org/10.1029/2004GL020051

Guerin F, Laforte C, Farinas MI, Perron J (2016) Analytical model based on experimental data of centrifuge ice adhesion tests with different substrates. Cold Reg Sci Technol 121:93–99. https://doi.org/10.1016/j.coldregions.2015.10.011

Huang SB, Liu QS, Liu YZ, Ye ZY, Cheng AP (2018) Freezing strain model for estimating the unfrozen water content of saturated rock under low temperature. Int J Geomech 18(2):04017137. https://doi.org/10.1061/(ASCE)GM.1943-5622.0001057

Jellinek HHG (1959) Adhesive properties of ice. J Colloid Sci 14(3):268–280. https://doi.org/10.1016/0095-8522(59)90051-0

Jia H, Leith K, Krautblatter M (2017) Path-dependent frost-wedging experiments in fractured, low-permeability granite. Permafr Periglac Process 28:698–709. https://doi.org/10.1002/ppp.1950

Jia H, Ding S, Wang Y, Zi F, Sun Q, Yang G (2019) An NMR-based investigation of pore water freezing process in sandstone. Cold Reg Sci Technol 168:102893. https://doi.org/10.1016/j.coldregions.2019.102893

Jia H, Zi F, Yang G, Li G, Shen Y, Sun Q, Yang P (2020) Influence of pore water (ice) content on the strength and deformability of frozen argillaceous siltstone. Rock Mech Rock Eng 53:967–974. https://doi.org/10.1007/s00603-019-01943-0

Kodama N, Fujii Y, Akagawa S, Ishijima Y (2007) Changes in mechanical properties and deformation behaviors of rocks due to freezing of pore water. J Jpn Soc Civ Eng Ser C 63(1):24–33

Kodama J, Goto T, Fujii Y, Hagan P (2013) The effects of water content, temperature and loading rate on strength and failure process of frozen rocks. Int J Rock Mech Min Sci 62:1–13. https://doi.org/10.1016/j.ijrmms.2013.03.006

Kodama JI, Mitsuib Y, Harac S, Fukudaa D, Fujiia Y, Sainokid A, Karakus M (2019) Time-dependence of mechanical behavior of Shikotsu welded tuff at subzero temperatures. Cold Reg Sci Technol 168:102868. https://doi.org/10.1016/j.coldregions.2019.102868

Kurilko AS, Novopashin MD (2005) Features of low temperature effect upon strength of enclosing rock and kimberlite in the "Udachnaya" pipe. J Min Sci 41:119–122. https://doi.org/10.1007/s10913-005-0071-7

Martinez GA, Davis LA (2000) Petrophysical measurements on shales using NMR. In SPE/AAPG Western Regional Meeting. https://doi.org/10.2118/62851-MS

Matsuoka N, Murton J (2008) Frost weathering : recent advances and future directions. Permafrost Periglac Process 19(2):195–210. https://doi.org/10.1002/ppp.620

Matteson A, Tomanic JP, Herron MM, Allen DF, Kenyon WE (1998) NMR relaxation of clay-brine mixtures. In SPE Annual Technical Conference and Exhibition. . https://doi.org/10.2118/49008-ms.

Meiboom S, Gill D (1958) Modified spin-echo method for measuring nuclear relaxation times. Rev Sci Instrum 29:688–691. https://doi.org/10.1063/1.1716296

Ondrášik M, Kopecký M (2014) Rock pore structure as main reason of rock deterioration. Stud Geotech Mech 36(1):79–88. https://doi.org/10.2478/sgem-2014-00102014-0010

Rempel AW (2007) Formation of ice lenses and frost heave. J Geophys Res Earth Surf 112:F02S21. https://doi.org/10.1029/2006JF000525

Shen YJ, Wang YZ, Yang Y, Sun Q, Luo T, Zhang HM (2019) Influence of surface roughness and hydrophilicity on bonding strength of concrete-rock interface. Constr Build Mater 213:156–166. https://doi.org/10.1016/j.conbuildmat.2019.04.078

Tice AR, Anderson DM, Sterrett KF (1982) Unfrozen water contents of submarine permafrost determined by nuclear magnetic resonance. Dev Geotech Eng 28:35–146. https://doi.org/10.1016/B978-0-444-42010-7.50017-7

Vlahou I, Worster MG (2010) Ice growth in a spherical cavity of a porous medium. J Glaciol 56:271–277. https://doi.org/10.3189/002214310791968494

Watanabe K, Mizoguchi M (2002) Amount of unfrozen water in frozen porous media saturated with solution. Cold Reg Sci Technol 34:103–110. https://doi.org/10.1016/S0165-232X(01)00063-5

Watanabe K, Wake T (2009) Measurement of unfrozen water content and relative permittivity of frozen unsaturated soil using NMR and TDR. Cold Reg Sci Technol 59(1):34–41. https://doi.org/10.1016/j.coldregions.2009.05.011

Weng L, Wu ZJ, Liu QS, Wang ZY (2019) Energy dissipation and dynamic fragmentation of dry and water-saturated siltstones under sub-zero temperatures. Eng Fract Mech 220:106659. https://doi.org/10.1016/j.engfracmech.2019.106659

Weng L, Wu ZJ, Liu QS (2020) Dynamic mechanical properties of dry and water-saturated siltstones under sub-zero temperatures. Rock Mech Rock Eng 53:4381–4401. https://doi.org/10.1007/s00603-019-02039-5

Yamabe T, Neaupane KM (2001) Determination of some thermo-mechanical properties of Sirahama sandstone under subzero temperature condition. Int J Rock Mech Min Sci 38(7):1029–1034. https://doi.org/10.1016/S1365-1609(01)00067-3

Yang GS, Xi JM, Li HJ, Cheng L (2010) Experimental study of rock mechanical properties under triaxial compressive and frozen conditions. Chin J Rock Mech Eng 29(3):459–464

Yoshikawa K, Overduin PP (2005) Comparing unfrozen water content measurements of frozen soil using recently developed commercial sensors. Cold Reg Sci Technol 42(3):250–256. https://doi.org/10.1016/j.coldregions.2005.03.001

Zhao Y, Sun Y, Liu S, Wang K, Jiang Y (2017) Pore structure characterization of coal by NMR cryoporometry. Fuel 190:359–369. https://doi.org/10.1016/j.fuel.2016.10.121

Zhou XH, Zhou J, Kinzelbach W, Stauffer F (2014) Simultaneous measurement of unfrozen water content and ice content in frozen soil using gamma ray attenuation and TDR. Water Resour Res 50:9630–9655. https://doi.org/10.1002/2014WR015640